Repository of the Max Delbrück Center for Molecular Medicine (MDC) in the Helmholtz Association

Schizophrenia risk candidate protein ZNF804A interacts with STAT2 and influences interferon-mediated gene transcription in mammalian cells

Klockmeier K., Silva Ramos E., Raskó T., Martí Pastor A., Wanker E.E.

Schizophrenia risk candidate protein ZNF804A interacts with STAT2 and influences interferon-mediated gene transcription in mammalian cells

Konrad Klockmeier[1*], Eduardo Silva Ramos[1*], Tamás Raskó[2], Adrián Martí Pastor[1], and Erich E. Wanker[1,3]

[1]Max-Delbrück-Center for Molecular Medicine in the Helmholtz Association (MDC), Laboratory for Neuroproteomics, Berlin, Germany

[2]Max-Delbrück-Center for Molecular Medicine in the Helmholtz Association (MDC), Laboratory for Mobile DNA, Berlin, Germany

[3]corresponding author

*Contributed equally

Family name

Correspondence: erich.w@mdc-berlin.de (E.E.W.)

Abstract

Previously evidence was presented that the single-nucleotide polymorphism rs1344706 located in an intronic region of the *ZNF804A* gene is associated with reduced transcript levels in fetal brains. This genetic variation in the gene encoding the zinc-finger protein ZNF804A is associated with schizophrenia (SZ) and bipolar disorder. Currently, the molecular and cellular function of ZNF804A is unclear. Here, we generated a high-confidence protein-protein interaction (PPI) network for ZNF804A using a combination of yeast two-hybrid and bioluminescence-based PPI detection assays, directly linking 12 proteins to the disease-associated target protein. Among the top hits was the signal transducer and activator of transcription 2 (STAT2), an interferon-regulated transcription factor. Detailed mechanistic studies revealed that STAT2 binds to the unstructured N-terminus of ZNF804A. This interaction is mediated by multiple short amino acid motifs in ZNF804A but not by the conserved C2H2 zinc-finger domain, which is also located at the N-terminus. Interestingly, investigations in HEK293 cells demonstrated that ZNF804A and STAT2 both co-translocate from the cytoplasm into the nucleus upon interferon (IFN) treatment. Furthermore, a concentration-dependent effect of ZNF804A overproduction on STAT2-mediated gene expression was observed using a luciferase reporter, which is under the control of an IFN-stimulated response element (ISRE). Together these results indicate the formation of ZNF804A:STAT2 protein complex and its translocation from the cytoplasm into the nucleus upon IFN stimulation, suggesting that it may function as a signal transducer that activates IFN-mediated gene expression programs.

Introduction

Schizophrenia (SZ) is a common neuropsychiatric disorder with a complex etiology and a worldwide prevalence of ~0.4% [1]. Currently, only symptomatic treatments are available for SZ, which partially improve disease symptoms [2,3]. Thus, a better understanding of the underlying disease mechanism is of crucial importance for the development of more precise, disease modifying therapies.

In recent genome-wide association studies (GWAS) more than 100 chromosomal loci with genetic variants have been identified to be associated with SZ [4]. This supports the view that SZ is a complex neurological disease and multiple risk candidates influence onset and progression of disease [5,6]. One of the top single-nucleotide polymorphisms (SNPs) associated with SZ is rs1344706, which is located in intron 2 in the *ZNF804A* gene on chromosome 2q31.1 [4]. The SNP rs1344706 has been associated with reduced transcript expression of full-length or of a splice variant of *ZNF804A* in fetal brain [7–9]. This suggests that perturbation of *ZNF804A* gene function in neurons contributes to disease development. Importantly, genetic variants in the *ZNF804A* gene locus were also found to be associated with the development other psychiatric diseases such as bipolar disorder [10], indicating that perturbation of *ZNF804A* gene function may influence multiple disease phenotypes.

Experimental evidence was provided that the rs1344706 genotype has a significant effect on *ZNF804A* gene expression in fetal brain [9], proposing that changes in mRNA transcript levels during brain development might contribute to the SZ disease phenotype. In addition, rs1344706-associated changes in *ZNF804A* transcript isoforms and transcript levels were observed in independent studies [8], supporting the hypothesis that proper *ZNF804A* gene expression is critical for normal brain function and development. However, the

molecular mechanism by which the intronic SNP rs1344706 influences *ZNF804A* mRNA levels in neurons is currently not sufficiently understood.

The *ZNF804A* gene encodes a largely unstructured protein that contains two central nuclear localization signals (NLS) and a well-conserved N-terminal C2H2 zinc-finger domain [11]. Zinc fingers are structural motifs that often function as DNA binding and interaction modules [12], suggesting that ZNF804A interacts with DNA and influences gene expression in neurons. This view is also supported by experimental evidence, indicating that ZNF804A is located in the nucleus, directly binds to DNA and influences transcription of multiple target genes [13,14,14,15]. However, further studies also showed that ZNF804A in neurons is present in the cytoplasm [16] as well as in synapses and regulates neurite formation [17], indicating that it has a cellular function in extranuclear compartments that is distinct from its role in gene expression in the nucleus. The observation that knock-down (KD) of ZNF804A in neurons results in loss of spine density and impairment of responses to activity-dependent stimulation [17] are consistent with clinical observations in brains of SZ patients and support the hypothesis that impairment of synapse function plays a critical role in disease [18–20]. Whether alterations of nuclear or extranuclear ZNF804A functions in neurons are responsible for the observed clinical manifestations in disease, however, remain unclear.

Here, genome-wide yeast two-hybrid screening and further validation using DULIP (dual luminescence-based co-immunoprecipitation) and BRET (bioluminescence resonance energy transfer) in mammalian cells revealed a high-confidence protein-protein interaction (PPI) network linking 12 new and previously reported protein interactors directly to ZNF804A. Among the top hits was the signal transducer and activator of transcription 2 (STAT2), an interferon-regulated transcription factor. A peptide array of the N-terminus of ZNF804A revealed multiple STAT2 binding sites downstream of ZNF804A's zinc-finger domain. We

further demonstrated that endogenous ZNF804A together with its interaction partner STAT2 co-translocate from the cytoplasm into the nucleus upon interferon (IFN2α) treatment. Interestingly, co-overexpression of STAT2 and ZNF804A results in the formation of distinct perinuclear clustered foci in mammalian cells. Furthermore, using an IFN-stimulated response element (ISRE) assay, we show that STAT2 can bind to the ISRE promoter and mediates expression of a luciferase reporter. This STAT2-mediated gene expression was attenuated in a dose- and interaction-dependent manner by increased ZNF804A expression. These results suggest that ZNF804A may act as an IFN-stimulated transcription regulator through its interaction with STAT2 in mammalian cells. The potential relevance of these findings for the development of SZ in patients that contain SNPs such as rs1344706 in *ZNF804A* gene locus are discussed.

Results

Yeast two-hybrid screening identifies ZNF804A putative protein interaction partners

A near genome-wide yeast two-hybrid (Y2H) screen was performed to determine the protein-protein interactome of human ZNF804A. As an initial primary screen, 16,888 prey proteins were tested against full-length and two ZNF804A fragments (1-609, 601-1209) as bait proteins (Figure 1A, asterisks). In our Y2H screen, the bait proteins were tagged with a LexA DNA-binding domain N- or C-terminally and expressed in a *L40ccua* MATa yeast strain, while prey proteins are tagged with a nuclear localization signal and a Gal4 activation domain N- or C-terminally and expressed in a MATα yeast strain (Figure 1B). Automated Y2H screenings were repeated four times on selective media (SDIV) and nylon membranes placed on SDIV media. A confidence scoring system was developed using experimental reproducibility (at least 3 times repeated growth of yeast colonies on selective SDIV media

and repeated activation of the LacZ reporter) to select for Y2H interactions. Through our systematic high-throughput mating of MATa bait and MATα prey yeast strains we identified 84 positive colonies that reconstituted the transcription factor to express the auxotrophy genes (*HIS3* and *URA3*) required for cell survival on selective plates. Of these positive colonies, 11 proteins were positive with N-terminal ZNF804A, 42 proteins interacted with C-terminal ZNF804A, and 39 proteins interacted with full-length ZNF804A (Supplementary Figure 1).

Due to the immense size of the primary screen (204,000 PPIs tested), additional control experiments were not performed. Therefore, the 80 initial hits were rescreened with more stringent parameters to control for successful mating and false positives (Figure 1C). We also included four additional ZNF804A N- and C-terminal bait fragments of varying sizes to better define interaction regions (Figure 1A). Each bait-prey pairing (4 orientations) was performed as quadruplicates for a total of 9,408 PPIs tested. Interacting bait-prey pairs were identified through growth selection on SDIV medium and successful mating controlled by assessing growth on SDII medium. A bait-prey interaction on SDIV plates was considered positive when at least eleven out of the sixteen matings survived (4 orientations x 4 replicates). As a further control, false positives were determined by assessing auto-activation of prey strains when mated with MATα strains producing only GAL4 or GAL4-mCherry. Conversely, ZNF804A bait strains were tested against MATa strains expressing LexA or LexA-mCherry. None of the ZNF804A bait strains displayed auto-activation. Lastly, the identity of preys in positively mated colonies was determined by Sanger sequencing.

After these extensive control experiments, our secondary Y2H screen identified 18 high-confidence ZNF804A interactors. Overall, the C-terminus of ZNF804A was a major area for PPIs accounting for 17 out of the 18 Y2H hits (Figure 2A and Supplementary Figure 2). STAT2, a transcription factor involved in the signal transduction pathway of type I interferons,

was the only protein that interacted with N-terminal ZNF804A fragments harboring the zinc finger domain (Figure 2A). Interestingly, in contrast to our primary screen, we were unable to replicate interactions with full-length ZNF804A in the secondary Y2H screen (Supplementary Figure 2). Manual literature curation revealed a prevalent group of proteins among the Y2H hits representing RNA binding proteins (DAZAP2, FAM46A, QKI, RBM4, RBM4B, and RBM46), suggesting a potential role for ZNF804A in gene expression (Figure 2B). Interestingly, a second large functional group of proteins (DAZAP2, EYA3, RBM4, RBM4B, STAT2 and TSC1) are described to play a role in the circadian rhythm (Figure 2B). Circadian rhythm disturbance is a common feature in psychiatric disorders, especially in SZ [21]. A third group of proteins represented among the Y2H hits have been associated with immune system regulation (LITAF, DAZAP2, TCS1, STAT2) (Figure 2B).

To evaluate the association with SZ of identified ZNF804A interactors, we used the Schizophrenia Gene Resource 2 (SZGR2) Database, which contains schizophrenia associated genes from multiple datasets for common variants, *de novo* mutations, copy number variants, differentially expressed genes and differentially methylated genes [22]. The 18 Y2H hits were cross-referenced in the SZGR2 database to determine their association with SZ. We found over 60% of identified ZNF804A PPI partners (DAZAP2, EYA3, KRTAP19-7, LASP1, PTS, QKI, RBM4, RBM4B, SEMA4G, STAT2, STAM2 and UBC9) to be associated with SZ (Figure 2B and Supplementary Table 1). Additionally, we performed a set-based test of all 18 Y2H hits using the dataset from the large SZ genetic study PGC2 GWAS [4]. We found most of these genes associated with SZ through at least one SNP in the PGC2 GWAS dataset; however, only with nominal significance (Supplementary Table 2). The protein Quaking (QKI), involved in mRNA processing, was the only ZNF804A interactor showing a significant enrichment of SNPs in the PGC2 GWAS set when correcting for the set of 18 interactors instead of the whole genome

(Supplementary Table 2). Overall, we identified 18 high-confidence PPIs for ZNF804A by whole genome Y2H screening and classify over 60% to be SZ-associated underlining the impact of ZNF804A in SZ.

DULIP and BRET approaches validate 67 % of identified Y2H ZNF804A interactors

The 18 PPIs identified by Y2H screening were further validated using two independent and quantitative binary PPI methods in mammalian cells. We have previously shown that DULIP and BRET assays are valuable PPI interaction mapping methods that both quantitatively and sensitively detect transient and stable binary interactions with high validation rates [23,24]. The DULIP assay is based on the co-immunoprecipitation of Firefly luciferase-tagged prey proteins by protein A Renilla luciferase-tagged bait proteins. The workflow for DULIP requires the co-transfection of prey and bait plasmids into HEK293 cells, allowing for the abundant production of luciferase-tagged proteins (Figure 3A). This is followed by co-immunoprecipitation and luciferase readout of precipitated interacting proteins to obtain normalized interaction ratios (cNIRs). This ratio can be used as an indication of binding strength, allowing for the distinction between high and low affinity interactions [23]. In our DULIP screen, STAT2 was screened against ZNF804A 1-400 and all other interaction candidates were screened against ZNF804A 800-1209 fragments as bait and prey proteins, as discovered by Y2H screening. Based on our previous benchmarking with positive and negative reference sets, a cNIR cutoff of ≥3 was determined to be a suitable threshold for significance [23]. Here, we selected a stringent cNIR score of ≥4 to distinguish positive PPIs from potential false-positives. Under these conditions 14 out of 18 (77%) tested Y2H interactions were validated with DULIP using C- and N-terminal fragments of ZNF804A as baits and preys (Figure 3B and E). RBM46 and STAT2 displayed the highest cNIR scores, suggesting them as high

affinity ZNF804A interactors (Figure 3B). FAM68 and STAM2 also exhibited high cNIR scores, followed by KRTAP19-7, QKI, DAZAP2, KRATP19-1, TSC1, RBM4, KRTAP8-1, LITAF, RBM4B, and PTS (Figure 3B and E).

An unexpected result from our secondary Y2H screen was the lack of positive interactions with full-length ZNF804A. To gain insights into whether the 18 Y2H hits interact with full-length ZNF804A in mammalian cells, we utilized the in-cell BRET assay reported previously to be a critical component of the LuTHy (bioluminescence-based two-hybrid) method (Figure 3C) [24]. We have previously shown that our in-cell BRET method using nanoluciferase (NanoLuc) and mCitrine as donor and acceptor pairs can quantitatively detect transient and stable PPIs using full-length proteins [24]. In contrast to DULIP, BRET assays measure PPIs in intact cells using the brighter NanoLuc (compared to Firefly luciferase). In our assays, we screened full-length ZNF804A fused to NanoLuc against all 18 with Y2H identified PPI partners fused to mCitrine-PA in triplicates and in 4 independent repetitions (Figure 3C). Similar to DULIP, normalized BRET efficiency (cBRET) values were determined for all tested interactions. Based on our previous benchmarking with positive and negative reference sets, a cBRET cutoff of ≥0.01 was determined to be a suitable threshold for significance [24]. Here, we selected an even more stringent cBRET score of ≥0.02 to distinguish positive PPIs from potential false-positives. Based on this cutoff, a total of 8 out of 18 interactions (44%) were successfully validated with in-cell BRET measurements (Figure 3D). Taken together, 15 out of 18 interactions were successfully validated with DULIP and/or BRET assays, representing a validation rate of 83% (Figure 3E). Seven proteins (FAM46A, KRTAP19-1, KRTAP8-1, PTS, RBM4, RBM4B, STAT2) were validated with both binary approaches, suggesting that these proteins are highly-relevant ZNF804A interactors (Figure 3E).

STAT2 interacts with several N-terminal ZNF804A regions

Of particular interest from our PPI data is the interaction between ZNF804A and STAT2. Not only was it the only interactor found positive with the N-terminal region containing the zinc-finger domain of ZNF804A, but it also exhibited a high DULIP cNIR score with ZNF804A fragments and was found to interact with the full-length protein. STAT2 is a transcription factor critical for signal transduction of type I interferons [25]. It resides primarily in the cytoplasm and upon IFNα/β treatment of cells, it homo or hetero dimerizes with STAT1, binds to IRF9, and finally translocates into the nucleus where it initiates the expression of viral response genes [26]. Considering that STAT2 is associated with SZ and that the immune system may play a central role in SZ [22,27], we proceeded to characterize the ZNF804A-STAT2 interaction in more depth.

To elucidate potential critical amino acids in the N-terminal binding domain of ZNF804A that interacts with STAT2 an INVATIS Celluspot peptide array composed of various peptide lengths from the first 400 amino acids was utilized. This protein region was divided into 40 sections with each section containing 15 residue peptides, of which 5 residues overlapped to the adjacent section (Supplementary Table 3). As a STAT2 positive control, the interferon regulatory factor 9 (IRF9), a known STAT2 binding partner, was also peptide arrayed (amino acids 205-393, 19 sections) in a similar fashion as ZNF804A (Supplementary Table 3). Recombinant human STAT2 was then applied to the arrays and binding to peptides detected by immunoblotting. The specificity of the STAT2 antibody (Santa Cruz, sc-476) was tested against all seven members of the STAT family in HEK293 cells transiently expressing N-terminal GFP fusion proteins. For all samples, endogenous STAT2 was detected at 113 kDa and only GFP-STAT2 transfected cell samples exhibited an additional band at the expected size for GFP-STAT2 (Figure 4A). Furthermore, we confirmed that our STAT2 antibody can

detect recombinant STAT2 protein (Figure 4B). To rule out peptides that may exhibit promiscuous protein binding, both ZNF804A and IRF9 arrays were tested against recombinant mCherry. No specific binding interaction was observed between mCherry and arrayed peptides from the proteins ZNF804 or IRF9 (Supplementary Figure 3). However, when STAT2 was applied to the ZNF804A array, three distinct peptides (#21, 25, and 31) downstream of the zinc-finger domain displayed pronounced STAT2 binding (Figure 4C and E). Several other ZNF804A peptides (#1-3, 6-9, 12, 14, and 34) also showed mild STAT2 reactivity (Figure 4C). Additionally, STAT2 showed an expected strong binding reactivity to several IRF9 peptides (#42, 47, 48, 52, and 53) spanning multiple peptide spots indictive of an interaction motive (Figure 4C). Interestingly, the peptide array suggests that the zinc-finger domain in ZNF804A does not contribute to the binding between ZNF804A and STAT2. To investigate this further we performed a BRET assay with a ZNF804A 1-400 fragment containing or lacking the zinc-finger domain as the donor protein and STAT2 as the acceptor. We found that the lack of the zinc-finger domain does not affect STAT2 binding (Figure 4D). These data demonstrate that STAT2 has multiple interaction interfaces with ZNF804A, which is in agreement with the high binding affinity (cNIR score) observed in DULIP experiments.

STAT2 binds primarily to unstructured domains of ZNF804A

Currently there is no available crystal structure of ZNF804A to map the STAT2 binding areas detected in our peptide array. To circumvent this, we first assessed the biochemical properties of ZNF804A peptides. Using the GenScript peptide property calculator tool, two ZNF804A peptides (#21, #25) with strong binding reactivity to STAT2 were found to be highly ionic and having isoelectric points of 9.69 and 12.53 respectively (Figure 4F). This would suggest that the interaction between STAT2 and ZNF804A may be dependent on ionic

strength. In order to gain structural insights of ZNF804A, we performed a predictive structural analysis using PredictProtein [28]. Through this approach, we found the N-terminal domain in ZNF804 is largely unstructured, except for the zinc-finger domain (Figure 4G). In regard to the peptides with strong STAT2 binding reactivity, two (#25 and #31) were found located within a predicted unstructured region, while one peptide (#21) partially overlapped with a potential strand region (Figure 4G).

ZNF804A and STAT2 co-migrate into the nucleus after IFN2α treatment

To analyze the interaction between ZNF804A and STAT2 in a cellular context, we performed immunocytochemistry on fixed human neuroblastoma SHEP cells followed by confocal microscopy. Immunostaining for the endogenous proteins showed that both are localized mainly in the cytosol (Figure 5A). Furthermore, line scan analysis revealed substantial fluorescent overlap in the cytosol between the two proteins (Figure 5B). It is well-established that, upon interferon α or β induction, STAT2 translocates to the nucleus and acts as a transcription factor [25]. Based on our PPI data, we hypothesized that ZNF804A would translocate with STAT2 upon IFN2α treatment. To evaluate this, we treated SHEP cells for 6 hours with 100 U/ml IFN2α and analyzed their localization. Indeed, we observed the translocation of both STAT2 and ZNF804A into the nucleus after IFN2α treatment (Figure 5A). Further line scan analysis revealed a high degree of fluorescent overlap in the nucleus between the two proteins (Figure 5B). This finding not only supports the interaction data between ZNF804A with STAT2 but also gives a strong indication that both proteins are functionally linked.

Overexpression of ZNF804A and STAT2 lead to the formation of perinuclear speckles

To better understand the interplay of STAT2 and ZNF804A we co-transfected constructs encoding mCherry-ZNF804A and GFP-STAT2 into SHEP cells. Confocal microscopy on fixed samples revealed that co-expression of GFP-STAT2 and mCherry-ZNF804A led to an accumulation of perinuclear speckles that displayed a high degree of co-localization between the two overexpressed proteins (Figure 5C and D). However, transfection of mCherry-ZNF804A or GFP-STAT2 alone did not result in the appearance of perinuclear accumulations (Figure 5C). This suggests that perinuclear aggregates are the result of a STAT2:ZNF804A interaction due to protein overexpression. To substantiate this finding, we performed filter retardation experiments with cells transfected with GFP-STAT2 and different concentrations of mCherry-ZNF804A or mCherry. Immunoblotting with STAT2 antibody revealed a concentration ZNF804A-dependent increase of STAT2 in aggregates (Figure 5E and F). In contrast, we did not detect a concentration mCherry-dependent increase of STAT2 (Figure 5E and F), indicating that perinuclear accumulation is specific for the interaction between STAT2 and ZNF804A.

ZNF804A overexpression modulates STAT2 activity in IFN2α -stimulated HEK293 cells

Our studies indicate that ZNF804A overproduction leads to abnormal STAT2 aggregation in perinuclear structures (Figure 5C-F), suggesting that overexpression of ZNF804A might also have a dominant negative effect on STAT2 function, which plays a role in gene expression regulation [25]. To evaluate the potential impact of ZNF804A overproduction on STAT2 function and IFN2α signaling [25], we studied STAT2 activity in HEK293 cells using an IFN-stimulated response element (ISRE) reporter assay (Figure 6A). The ISRE reporter assay utilizes two luciferases, Firefly luciferase under the control of the ISRE promoter and Renilla luciferase which is constitutively active. Upon IFN2α treatment, STAT2 should translocate

from the cytoplasm into the nucleus and bind to the ISRE element, leading to expression of Firefly luciferase (Figure 6A). This two-readout strategy allows the evaluation of changes in ISRE activation while eliminating the effects of different transfection efficiencies and cell numbers. We first evaluated the response to 24-hour IFN2α treatment with increasing concentrations of IFN2α and determined an effective concentration of 50 U/ml for half-maximal reporter gene activation (Figure 6B). We applied this concentration of IFN2α in all further experiments in order to identify potential changes in reporter response. Next, plasmids encoding mCherry-tagged full-length ZNF804A or N-and C-terminally truncated fragments (1-400 and 800-1209) were transfected together with the reporter constructs. Cells were then incubated for 48 hours and 50 U/ml of IFN2α was applied. Finally, after additional incubation for 24 hours Firefly and Renilla luciferase activities were quantified. For all ZNF804A constructs transfected, we did not observe a significant change in ISRE reporter activity (Figure 6C), indicating that overproduction of different ZNF804A proteins alone does not significantly change reporter activity in IFN2α treated cells. In strong contrast, when a construct encoding GFP-STAT2 was co-transfected together with the reporter plasmid, we found a ~4-fold increase in ISRE reporter activity after IFN2α treatment (Figure 6C), indicating that STAT2 overproduction, as expected [25], robustly induces reporter gene expression under these experimental conditions. Strikingly, we observed that GFP-STAT2-mediated activation of reporter gene expression was significantly reduced when full-length ZNF804A or a N-terminal fragment (1-400) were co-expressed in HEK293 cells (Figure 6C), indicating that ZNF804A-mediated GFP-STAT2 aggregation in the cytoplasm (Figure 5C-F) decreases IFNα-stimulated reporter gene activation. However, no such effect on reporter gene expression was observed, when an N-terminally truncated ZNF804A fragment (800-1209) lacking the STAT2 interaction domain was applied, demonstrating that a direct interaction between

ZNF804A and STAT2 is critical for modulation of reporter activity. These results were also confirmed in independent experiments, when increasing concentrations of mCherry-tagged ZNF804A were co-expressed together with GFP-STAT2 in ISRE reporter cells (Figure 6D).

Discussion

Multiple genome-wide association studies indicate that *ZNF804A* is a risk gene for SZ [10,29]. The cellular function of the SZ-associated zinc-finger protein ZNF804A and its specific role in disease, however, are still unclear. Here, utilizing quantitative PPI mapping technologies, we discovered multiple high-confidence interaction partners that directly bind to ZNF804A in mammalian cells (Figure 2). Among these binding proteins, we found that the protein STAT2 directly interacts with the N-terminus of ZNF804A but does not bind to the conserved N-terminal zinc-finger domain. STAT2 functions as a signal transducer that activates gene transcription in cells, when treated with interferons (IFNs) such as IFNα or IFNγ [30]. In untreated cells, STAT2 is predominantly located in the cytoplasm; however, upon IFN treatment an active signaling complex consisting of the proteins STAT1, STAT2 and IRF9 is rapidly formed, which translocates into the nucleus, binds to promoters, and activates the transcription of over 300 target genes [25]. This 'canonical' IFN-stimulated signaling pathway is known for more than 20 years and is commonly activated in response to bacterial and viral infections of cells [31]. Thus, the process of IFN-mediated JAK-STAT signaling is a critical defense mechanism required for the survival of mammalian cells [32].

Our data indicate that upon IFN2α stimulation of SHEP cells, STAT2 directly interacts with ZNF804A in the cytoplasm and then translocates as a protein complex into the nucleus and activates gene expression (Figure 5 and 6). This suggests that ZNF804A together with STAT2 plays a functional role in a 'non-canonical' IFN-mediated JAK-STAT signaling pathway.

Our data are in agreement with previously reported observations, indicating that ZNF804A in neurons is present both in the cytoplasm and the nucleus [17] as well as that it contains two putative nuclear localization signals. However, to this day it has not been shown that ZNF804A can translocate from the cytoplasm into nucleus in cells upon IFN2α treatment.

Based on our studies, we propose that ZNF804A and STAT2 form an IFN-induced transcription factor complex in neurons. However, additional studies are needed to better define this complex and to elucidate its specific role in IFN-induced transcription. For example, it needs to be assessed whether STAT2 phosphorylation or homo- or heterooligomerization are critical for ZNF804A binding. In the 'canonical' pathway IFN-mediated phosphorylation of STAT1 at Thy701 and of STAT2 at Tyr690 were shown to induce heterodimerization, which subsequently stimulates the interaction with IRF9 [33]. A similar mechanism may also be critical for ZNF804A binding to STAT2 and transcription activation. Also, it will be key to map the ZNF804A binding domain in STAT2. Previous investigation indicates that a coiled-coil domain in STAT2 mediates the interaction with IRF9 [25]. We hypothesize that this domain is also important for the association with ZNF804A. However, more detailed investigations of the STAT2:ZNF804A protein complex and its specific cellular functions are necessary using biochemical, structural and cell biological methods.

Our findings show that ZNF804A binds to STAT2 and influences IFN2α-induced transcription in cells. A connection between ZNF804A and IFN signaling has been observed before. For example, it was shown that knockdown (KD) of ZNF804A gene expression in neuronal progenitor cells (NPCs) leads to the down-regulation of a large number of transcripts encoding many proteins involved in IFN signaling [13]. In this study it was demonstrated that KD of ZNF804A reduces the expression of the genes *IFITM2* and *IFITM3*, which encode for IFN-induced transmembrane proteins that are well-known viral restriction factors [34]. They were

shown in independent studies to play a key role in protecting cells against the entry and replication of viruses [35]. In the context of the SZ the SNP rs1344706, it may influence the susceptibility to detrimental virus infections via the IFN-stimulated defense response by a yet undetermined regulatory process. This mechanism potentially is of high relevance because previous studies have provided evidence that maternal exposure to influenza and other viruses increases SZ risk in the offspring [36–38]. Thus, our results from PPI mapping studies and cell-based assays are supportive of reported experimental evidence indicating that prenatal virus infections increase the risk for developing SZ [37].

Finally, it is important to note that our results are also supported by a recently published very comprehensive analysis of RNAseq data of SZ patients and controls, indicating that the IFN response is significantly perturbed in SZ brains [39]. This analysis revealed a well-defined co-expression module (gene M32) that contains critical components of the IFN-stimulated gene factor 3 (ISGF3) complex that activates the transcription of downstream IFN-stimulated genes [39,40], supporting our hypothesis that molecular pathways that protect cells against viral infections are perturbed in SZ.

Based on our and previously reported studies, we suggest that treatment strategies that increase IFN signaling and thereby improve cellular virus defense mechanisms may improve cortical abnormalities in SZ brains. Interestingly, experimental evidence in rat cells treated with the chemical compound olanzapine increases the activity of the JAK-STAT signaling cascade [41], suggesting that this compound besides its other activities can activate cellular defense mechanisms against virus infections. Olanzapine is an atypical antipsychotic drug commonly used for the treatment of SZ and bipolar disorder [42].

Material and Methods

Yeast two-hybrid assay

The Y2H interaction mating assays were performed as previously published [43]. Briefly, bait constructs were transformed into yeast strains L40ccua (MATa) and for prey constructs a library of ~17,000 pre-transformed yeast L40ccα (MATα) strains was used. For interaction mating, MATα colonies grown on L-HAUT q-trays were robot spotted (KBiosystems) and mixed into 100 μl cultures of MATa yeast strains in 96-well microtiter plates. Yeast mixtures were then robot spotted onto YPD agar plates. After 48 hours of mating at 30°C, yeast colonies were transferred into 100 μl selective SDII (-Leu-Trp liquid medium) in 96-well microtiter plates using a spotting robot. For selection of PPIs, diploid yeasts were spotted onto SDIV (-Leu-Trp-Ura-His), as well as SDII (-Leu-Trp) selective agar plates. After incubation for 6 days at 30°C, agar plates were imaged, and yeast colony growth assessed.

Cell lines

Human embryonic kidney cell line 293 (HEK293) and a human neuroblastoma cell line (SHEP) were maintained in DMEM (Thermofisher, #41965) supplemented with 10% heat-inactivated fetal bovine serum (Thermofisher, #10500) and 1% penicillin/streptomycin (Thermofisher, #15140122) at 37°C and 5% CO_2. Cells were passaged every 3 to 4 days.

DULIP assay

HEK293 cells were reverse transfected with linear polyethyleneimine (25 kDa, Polysciences) in 96-well microtiter plates at a density of 3.5×10^4 cells per well. 48 h after transfection cells were lysed in 100 μl HEPES lysis buffer (50 mM HEPES, 150 mM NaCl, 10% glycerol, 1% NP-40, 0.5% deoxycholate, 20 mM NaF, 1.5 mM $MgCl_2$, 1 mM EDTA, 1 U Benzonase) for 30

minutes at 4°C. The amount of produced PA-Renilla and Firefly-tagged fusion proteins was monitored by measuring the respective luciferase activities in crude cell lysates in 384-well microtiter plates. To this end, 10 µl of cell lysate, 20 µl PBS, and 10 µl of Dual-Glo® luciferase reagent (Promega) was added to individual wells. After 10 minutes at 37°C the Firefly activity was measured using an Infinite® M1000 (Tecan) plate reader. In order to stop the Firefly luciferase activity and measure the Renilla luciferase activity, 10 µl of the Dual-Glo® Stop & Glow® reagent (Promega) were added, incubated for 15 minutes at 37°C and the activity was measured. Additionally, 50 µl of the cell lysate were incubated for 3 hours at 4°C in IgG pre-coated 384-well microtiter plates. Plates were pre-coated with sheep gamma globulin (Dianoca), blocked with 1% BSA in carbonate buffer (70 mM $NaHCO_3$, 30 mM Na_2CO_3, pH 9.6) for 1 h and then incubated with rabbit anti-sheep IgGs (Dianova) overnight at 4°C. After cell lysate incubation in antibody coated plates, all wells were washed three times with HEPES lysis buffer. Lastly, 10 ul of HEPES lysis buffer and 20 µl of PBS were added to each well and luminescence measurements for Firefly and Renilla were performed as described above. DULIP data were analyzed as described in the original publication [23].

BRET assay

HEK293 cells were reverse transfected with linear polyethyleneimine (25 kDa, Polysciences) in white 96-well microtiter plates at a density of 3.5 x10^4 cells per well. BRET assay was performed as previous described [24]. For low expressing ZNF804A donor constructs, DNA ratios of donor and acceptor were used at a 1:3 ratio, with 50 ng donor and 150 ng of acceptor. In other cases, a ratio of 1:10 was used, with 10 ng donor and 100 ng of acceptor. 48 h after transfection, mCitrine fluorescence was measured in intact cells with a Tecan Infinite® M1000Pro microtiter plate reader and at Ex/Em: 500 nm/530 nm. Afterwards, 5 µM

coelenterazine-h (NanoLight Technology, #301) was added and cells incubated for 10 min. NanoLuc emission was measured with the BLUE1 filter (370-480 nm), mCitrine emission due to BRET was measured using the GREEN1 filter (520-570 nm), and total luminescence without using a filter was also recorded using a Tecan Infinite® M1000Pro microtiter plate reader. The integration time for measurements was 100-1000 ms. BRET data were analyzed as previously described [24].

Immunocytochemistry

Coverslips were incubated with 10 µg/ml fibronectin (Sigma, F1141) and 10 µg/ml poly-L-lysine (Sigma, P8920) for 4 h at 37°C for coating. Coverslips were placed in a 24-well plate, SHEP cells were seeded ($7x10^4$ cells/well), and incubated overnight in DMEM (Thermofisher, #41965) supplemented with 10% heat-inactivated fetal bovine serum (Thermofisher, #10500) and 1% penicillin/streptomycin (Thermofisher, #15140122) at 37°C and 5% CO_2. The next day the cells transfected with 600 ng of plasmid for mCherry-ZNF804A, or GFP-STAT2, or co-transfected for 48 hours using GeneJet reagent according to manufacturer's instructions. For certain experiments, cells were treated with 100 U/ml of IFN2α (Sigma-Aldrich, I4276) for 6 hours at 37°C and 5% CO_2 prior to fixation. Cell were fixed with 2% PFA for 15 min at room temperature and treated with Hoechst 33342 (1:5000, Sigma) for 15 min. Coverslips were washed twice with 0.1% Triton-X in PBS (PBS-T). Cells were permeabilized for 10 min with PBS-T containing 1% BSA. Sample were blocked with PBS-T containing 1% BSA for 30 min. For experiments centered on imaging endogenous proteins, samples were incubated with rabbit anti-STAT2 (1:1000, Santa Cruz) and mouse anti-ZNF804A (1:1000, Synaptic Systems) for 1 h in the blocking solution. The coverslips were then washed three times with PBS-T and anti-mouse Alexa Fluor® 488 IgG (1:500, Ex_{495}/Em_{519}, Invitrogen) and anti-rabbit Alexa Fluor® 568

IgG (1:500, Ex_{578}/Em_{603}, Invitrogen) secondary antibodies diluted in the blocking solution were applied for 45 min at room temperature. Coverslips were washed three times with PBS-T and after a final wash with PBS, the coverslips were mounted with Dako fluorescence mounting medium (Dako) and dried overnight.

Imaging

Confocal microscopy. Fluorescence images were acquired using a laser-scanning Lecia TSC SP8 confocal microscope equipped with a diode, argon, and DPSS lasers. Images were acquired using sequential scanning and with z-stacks.

Image analysis. Colocalization analysis was performed using ImageJ software. A line scan analysis was performed on stacked confocal images acquired and analyzed using ImageJ. Using merged images, a line segment was drawn, the RGB profiler plugin applied, and spectra plots analyzed.

Western blotting

To analyze specificity of anti-STAT2 antibody for STAT2, HEK293 cells were transfected with pEGFP-C1 (Clontech) plasmids containing open reading frames for human STAT1, STAT2, STAT3, STAT4. STAT5a, STAT5b, or STAT6 using Lipofectamine 2000 according to manufacturer instructions. After 48 hours, cell pellets were lysed with HEPES buffer (50 mM HEPES, 150 mM NaCl, 10% glycerol, 1% NP-40, 0.5% deoxycholate, 20 mM NaF, 1.5 mM $MgCl_2$, 1 mM EDTA, 1 mM DTT, 1 U Benzonase, 1 mM PMSF, 25 mM glycerol-2-phosphate, 1 mM sodium orthovanadate) and protein concentration was measured using the BCA method (Thermofisher, #23228). A mixture of 25 µg of protein, 1x SDS-PAGE LDS Sample Buffer (ThermoFisher, #2165462) and 50 mM DTT was boiled at 95°C for 5 min and loaded on an

Invitrogen SDS-PAGE Bis-Tris 4-12% gels along with SeeBlue® Plus2 (Thermo-Fisher) as a size marker. Electrophoresis was performed at 185 V for 35 min with 1x MES SDS running buffer. Next, proteins were transferred onto a nitrocellulose membrane using wet blotting system with 1x Transfer buffer (25 mM Tris, 192 mM glycine, 10% methanol) at 100 V for 120 min. The membrane was blocked in 3 % milk with PBS containing 0.05% Tween 20 for 1 h at room temperature followed by overnight incubation at 4°C with primary antibody rabbit anti-STAT2 (1:20,000, Santa Cruz sc-476) in 3 % milk PBS-Tween. Membranes were washed three times with PBS-Tween and incubated with POD conjugated secondary anti-rabbit antibody (Sigma, A0545) at 1:2000 for 1 h at room temperature. Membranes were washed twice with PBS-Tween and once with PBS, and incubated with WesternBright Quantum (Advansta, K-12042) reagent. Chemiluminescence was acquired with a FujiFilm LAS-3000.

Dot blot assay

Dot blots were performed as previously described [44]. In brief, a nitrocellulose membrane with a pore size of 0.1 μm (Amersham Protran 0.1 μm NC, GE Healthcare Life Sciences, Munich, Germany) was washed once with PBS (13.7 mM NaCl, 0.27 mM KCl, 1 mM Na_2HPO_4, 0.2 mM KH_2PO_4, pH 7.4). Protein samples (25 μg, diluted in PBS) were spotted to membrane using a 96-well vacuum apparatus and membranes washed twice with PBS. Membrane was blocked for 30 min with 3% milk prepared with PBS containing 0.05% Tween 20. Membrane was incubated overnight at 4°C with rabbit anti-STAT2 antibody (1:1000, Santa Cruz sc-476) diluted in 3% milk PBS-Tween. Membrane was washed 3x with PBS-Tween and incubated with POD conjugated secondary anti-rabbit antibody at 1:2000 for 1 h at room temperature, followed by PBS-Tween washes, and incubation with ChemiGlow (Biozym, Hess. Oldendorf,

Germany). Chemiluminescence was acquired with a FujiFilm LAS-3000 and images quantified using the Aida image analysis software (Raytest, Straubenhardt, Germany).

Denaturing Filter Retardation Assay

To enable size-dependent retardation of insoluble proteins, samples were incubated with 2% SDS and 50 mM DTT for 5 min at 95°C and then filtered through a 0.2 µm cellulose acetate membrane preequilibrated in 0.1% SDS. The membrane was then washed with 0.1% SDS and immunoblotting performed as described for the dot blot assays.

ISRE assay

Cells were reverse transfected with linear polyethyleneimine (25 kDa, Polysciences) in 96 well plates with either 100 ng of each reporter construct (ISRE-Firefly, CMV-Renilla) and 100 ng of fusion protein constructs (GFP-STAT2, mCherry ZNF804A, mCherry ZNF804A 1-400, mCherry ZNF804A 800-1209). In the case where a single protein construct was transfected, 100 ng of pcDNA 3.1 was used to reached to total of 400 ng. 72 hours after transfection, cells were lysed using 20 µl HEPES lysis buffer (50 mM HEPES, 150 mM NaCl, 10% glycerol, 1% NP-40, 0.5% deoxycholate, 20 mM NaF, 1.5 mM $MgCl_2$, 1 mM EDTA, 1 mM DTT, 1 U Benzonase, 1 mM PMSF, 25 mM glycerol-2-phosphate, 1 mM sodium orthovanadate) for 30 minutes at 4°C. Firefly luminescence were measured by incubating lysates with 100 µl of Dual-Glo® luciferase reagent (Promega) After 10 minutes at 37°C Firefly activity was measured using an Infinite® M1000 (Tecan) plate reader. In order to stop the Firefly luciferase activity and measure the Renilla luciferase activity, 100 µl of the Dual-Glo® Stop & Glow® reagent (Promega) were added, incubated for 15 min at 37°C and the activity was measured. To assess relative Firefly expression, ratios of Firefly to Renilla were calculated for every well. As a negative control, a

Firefly luciferase plasmid lacking the ISRE promotor (tandem TRE) was co-transferred with the constitutively active Renilla luciferase. As a positive controls, the following pcDNA 3.1 constructs were co-transfected; GFP, Firefly, and Renilla. Lastly, the average value of technical replicates was calculated with standard deviations and normalized to the negative control. For certain experiments, cells were treated with 100 U/ml of IFN2α (Sigma-Aldrich, I4276) or increasing amounts of IFN2α for 6 hours at 37°C and 5% CO_2 before ISRE readouts were performed.

Peptide array

Ordered peptide arrays for human ZNF804A (Intavis) were blocked for 1 hour at room temperature with 3% milk prepared in PBS containing 0.05% Tween 20. Blocked peptide arrays were incubated with either 20 μl HIS-STAT2, HIS-mCherry or no additional protein, each in 3% milk PBS-Tween for overnight at 4°C. Afterwards, arrays were washed 3x with PBS-Tween for 10 min. Arrays were then immunoblotted with either rabbit anti-STAT2 (1:1000, Santa Cruz sc-476) or mouse anti-mCherry antibody (1:500, Clonetech 632543) in 3% milk PBS-Tween for 2 hours at room temperature. After washing 3x with PBS-Tween for 10 min, 3% milk with HRP fused secondary antibodies at 1:5000 was applied to arrays for 1 hour at room temperature. Arrays were then washed 2x with PBS-Tween and once with PBS, and WesternBright Quantum (Advansta, K-12042) was applied. Chemiluminescence was acquired with a FujiFilm LAS-3000.

References

[1] H. Jin, I. Mosweu, The Societal Cost of Schizophrenia: A Systematic Review, PharmacoEconomics. 35 (2017) 25–42. https://doi.org/10.1007/s40273-016-0444-6.

[2] U. Meyer, M.J. Schwarz, N. Müller, Inflammatory processes in schizophrenia: A promising neuroimmunological target for the treatment of negative/cognitive symptoms and beyond, Pharmacology & Therapeutics. 132 (2011) 96–110. https://doi.org/10.1016/j.pharmthera.2011.06.003.

[3] K.R. Patel, J. Cherian, K. Gohil, D. Atkinson, Schizophrenia: Overview and Treatment Options, P T. 39 (2014) 638–645.

[4] S. Ripke, B.M. Neale, A. Corvin, J.T.R. Walters, K.-H. Farh, P.A. Holmans, P. Lee, B. Bulik-Sullivan, D.A. Collier, H. Huang, T.H. Pers, I. Agartz, E. Agerbo, M. Albus, M. Alexander, F. Amin, S.A. Bacanu, M. Begemann, R.A. Belliveau Jr, J. Bene, S.E. Bergen, E. Bevilacqua, T.B. Bigdeli, D.W. Black, R. Bruggeman, N.G. Buccola, R.L. Buckner, W. Byerley, W. Cahn, G. Cai, D. Campion, R.M. Cantor, V.J. Carr, N. Carrera, S.V. Catts, K.D. Chambert, R.C.K. Chan, R.Y.L. Chen, E.Y.H. Chen, W. Cheng, E.F.C. Cheung, S. Ann Chong, C. Robert Cloninger, D. Cohen, N. Cohen, P. Cormican, N. Craddock, J.J. Crowley, D. Curtis, M. Davidson, K.L. Davis, F. Degenhardt, J. Del Favero, D. Demontis, D. Dikeos, T. Dinan, S. Djurovic, G. Donohoe, E. Drapeau, J. Duan, F. Dudbridge, N. Durmishi, P. Eichhammer, J. Eriksson, V. Escott-Price, L. Essioux, A.H. Fanous, M.S. Farrell, J. Frank, L. Franke, R. Freedman, N.B. Freimer, M. Friedl, J.I. Friedman, M. Fromer, G. Genovese, L. Georgieva, I. Giegling, P. Giusti-Rodríguez, S. Godard, J.I. Goldstein, V. Golimbet, S. Gopal, J. Gratten, L. de Haan, C. Hammer, M.L. Hamshere, M. Hansen, T. Hansen, V. Haroutunian, A.M. Hartmann, F.A. Henskens, S. Herms, J.N. Hirschhorn, P. Hoffmann, A. Hofman, M.V. Hollegaard, D.M. Hougaard, M. Ikeda, I. Joa, A. Julià, R.S. Kahn, L. Kalaydjieva, S. Karachanak-Yankova, J. Karjalainen, D. Kavanagh, M.C. Keller, J.L. Kennedy, A. Khrunin, Y. Kim, J. Klovins, J.A. Knowles, B. Konte, V. Kucinskas, Z. Ausrele Kucinskiene, H. Kuzelova-Ptackova, A.K. Kähler, C. Laurent, J. Lee Chee Keong, S. Hong Lee, S.E. Legge, B. Lerer, M. Li, T. Li, K.-Y. Liang, J. Lieberman, S. Limborska, C.M. Loughland, J. Lubinski, J. Lönnqvist, M. Macek Jr, P.K.E. Magnusson, B.S. Maher, W. Maier, J. Mallet, S. Marsal, M. Mattheisen, M. Mattingsdal, R.W. McCarley, C. McDonald, A.M. McIntosh, S. Meier, C.J. Meijer, B. Melegh, I. Melle, R.I. Mesholam-Gately, A. Metspalu, P.T. Michie, L. Milani, V. Milanova, Y. Mokrab, D.W. Morris, O. Mors, K.C. Murphy, R.M. Murray, I. Myin-Germeys, B. Müller-Myhsok, M. Nelis, I. Nenadic, D.A. Nertney, G. Nestadt, K.K. Nicodemus, L. Nikitina-Zake, L. Nisenbaum, A. Nordin, E. O'Callaghan, C. O'Dushlaine, F.A. O'Neill, S.-Y. Oh, A. Olincy, L. Olsen, J. Van Os, C. Pantelis, G.N. Papadimitriou, S. Papiol, E. Parkhomenko, M.T. Pato, T. Paunio, M. Pejovic-Milovancevic, D.O. Perkins, O. Pietiläinen, J. Pimm, A.J. Pocklington, J. Powell, A. Price, A.E. Pulver, S.M. Purcell, D. Quested, H.B. Rasmussen, A. Reichenberg, M.A. Reimers, A.L. Richards, J.L. Roffman, P. Roussos, D.M. Ruderfer, V. Salomaa, A.R. Sanders, U. Schall, C.R. Schubert, T.G. Schulze, S.G. Schwab, E.M. Scolnick, R.J. Scott, L.J. Seidman, J. Shi, E. Sigurdsson, T. Silagadze, J.M. Silverman, K. Sim, P. Slominsky, J.W. Smoller, H.-C. So, ChrisC.A. Spencer, E.A. Stahl, H. Stefansson, S. Steinberg, E. Stogmann, R.E. Straub, E. Strengman, J. Strohmaier, T. Scott Stroup, M. Subramaniam, J. Suvisaari, D.M. Svrakic, J.P. Szatkiewicz, E. Söderman, S. Thirumalai, D. Toncheva, S. Tosato, J. Veijola, J. Waddington, D. Walsh, D. Wang, Q. Wang, B.T. Webb, M. Weiser, D.B. Wildenauer, N.M. Williams, S. Williams, S.H. Witt, A.R. Wolen, E.H.M. Wong, B.K. Wormley, H. Simon Xi, C.C. Zai, X. Zheng, F. Zimprich, N.R.

Wray, K. Stefansson, P.M. Visscher, W. Trust Case-Control Consortium, R. Adolfsson, O.A. Andreassen, D.H.R. Blackwood, E. Bramon, J.D. Buxbaum, A.D. Børglum, S. Cichon, A. Darvasi, E. Domenici, H. Ehrenreich, T. Esko, P.V. Gejman, M. Gill, H. Gurling, C.M. Hultman, N. Iwata, A.V. Jablensky, E.G. Jönsson, K.S. Kendler, G. Kirov, J. Knight, T. Lencz, D.F. Levinson, Q.S. Li, J. Liu, A.K. Malhotra, S.A. McCarroll, A. McQuillin, J.L. Moran, P.B. Mortensen, B.J. Mowry, M.M. Nöthen, R.A. Ophoff, M.J. Owen, A. Palotie, C.N. Pato, T.L. Petryshen, D. Posthuma, M. Rietschel, B.P. Riley, D. Rujescu, P.C. Sham, P. Sklar, D. St Clair, D.R. Weinberger, J.R. Wendland, T. Werge, Schizophrenia Working Group of the Psychiatric Genomics Consortium, Psychosis Endophenotypes International Consortium, Biological insights from 108 schizophrenia-associated genetic loci, Nature. 511 (2014) 421–427. https://doi.org/10.1038/nature13595.

[5]   J. van Os, S. Kapur, Schizophrenia, The Lancet. 374 (2009) 635–645. https://doi.org/10.1016/S0140-6736(09)60995-8.

[6]   Y. Kim, S. Zerwas, S.E. Trace, P.F. Sullivan, Schizophrenia Genetics: Where Next?, Schizophr Bull. 37 (2011) 456–463. https://doi.org/10.1093/schbul/sbr031.

[7]   H. Chang, X. Xiao, M. Li, The schizophrenia risk gene ZNF804A: clinical associations, biological mechanisms and neuronal functions, Mol Psychiatry. 22 (2017) 944–953. https://doi.org/10.1038/mp.2017.19.

[8]   R. Tao, H. Cousijn, A.E. Jaffe, P.W.J. Burnet, F. Edwards, S.L. Eastwood, J.H. Shin, T.A. Lane, M.A. Walker, B.J. Maher, D.R. Weinberger, P.J. Harrison, T.M. Hyde, J.E. Kleinman, Expression of *ZNF804A* in Human Brain and Alterations in Schizophrenia, Bipolar Disorder, and Major Depressive Disorder: A Novel Transcript Fetally Regulated by the Psychosis Risk Variant rs1344706, JAMA Psychiatry. 71 (2014) 1112. https://doi.org/10.1001/jamapsychiatry.2014.1079.

[9]   M.J. Hill, N.J. Bray, Evidence That Schizophrenia Risk Variation in the ZNF804A Gene Exerts Its Effects During Fetal Brain Development, AJP. 169 (2012) 1301–1308. https://doi.org/10.1176/appi.ajp.2012.11121845.

[10]   M.C. O'Donovan, N. Craddock, N. Norton, H. Williams, T. Peirce, V. Moskvina, I. Nikolov, M. Hamshere, L. Carroll, L. Georgieva, S. Dwyer, P. Holmans, J.L. Marchini, C.C.A. Spencer, B. Howie, H.-T. Leung, A.M. Hartmann, H.-J. Möller, D.W. Morris, Y. Shi, G. Feng, P. Hoffmann, P. Propping, C. Vasilescu, W. Maier, M. Rietschel, S. Zammit, J. Schumacher, E.M. Quinn, T.G. Schulze, N.M. Williams, I. Giegling, N. Iwata, M. Ikeda, A. Darvasi, S. Shifman, L. He, J. Duan, A.R. Sanders, D.F. Levinson, P.V. Gejman, S. Cichon, M.M. Nöthen, M. Gill, A. Corvin, D. Rujescu, G. Kirov, M.J. Owen, Identification of loci associated with schizophrenia by genome-wide association and follow-up, Nature Genetics. 40 (2008) 1053–1055. https://doi.org/10.1038/ng.201.

[11]   J.L. Hess, S.J. Glatt, How might ZNF804A variants influence risk for schizophrenia and bipolar disorder? A literature review, synthesis, and bioinformatic analysis, American Journal of Medical Genetics Part B: Neuropsychiatric Genetics. 165 (2014) 28–40. https://doi.org/10.1002/ajmg.b.32207.

[12]   A. Klug, The Discovery of Zinc Fingers and Their Applications in Gene Regulation and Genome Manipulation, Annual Review of Biochemistry. 79 (2010) 213–231. https://doi.org/10.1146/annurev-biochem-010909-095056.

[13]   J. Chen, M. Lin, A. Hrabovsky, E. Pedrosa, J. Dean, S. Jain, D. Zheng, H.M. Lachman, ZNF804A Transcriptional Networks in Differentiating Neurons Derived from Induced Pluripotent Stem Cells of Human Origin, PLoS One. 10 (2015). https://doi.org/10.1371/journal.pone.0124597.

[14] M.J. Girgenti, J.J. LoTurco, B.J. Maher, ZNF804a Regulates Expression of the Schizophrenia-Associated Genes PRSS16, COMT, PDE4B, and DRD2, PLoS One. 7 (2012). https://doi.org/10.1371/journal.pone.0032404.

[15] M.J. Hill, A.R. Jeffries, R.J.B. Dobson, J. Price, N.J. Bray, Knockdown of the psychosis susceptibility gene ZNF804A alters expression of genes involved in cell adhesion, Human Molecular Genetics. 21 (2012) 1018–1024. https://doi.org/10.1093/hmg/ddr532.

[16] Y. Zhou, F. Dong, T.A. Lanz, V. Reinhart, M. Li, L. Liu, J. Zou, H.S. Xi, Y. Mao, Interactome analysis reveals ZNF804A , a schizophrenia risk gene, as a novel component of protein translational machinery critical for embryonic neurodevelopment, Molecular Psychiatry. 23 (2018) 952–962. https://doi.org/10.1038/mp.2017.166.

[17] P.J.M. Deans, P. Raval, K.J. Sellers, N.J.F. Gatford, S. Halai, R.R.R. Duarte, C. Shum, K. Warre-Cornish, V.E. Kaplun, G. Cocks, M. Hill, N.J. Bray, J. Price, D.P. Srivastava, Psychosis Risk Candidate ZNF804A Localizes to Synapses and Regulates Neurite Formation and Dendritic Spine Structure, Biological Psychiatry. 82 (2017) 49–61. https://doi.org/10.1016/j.biopsych.2016.08.038.

[18] I. Feinberg, Schizophrenia: Caused by a fault in programmed synaptic elimination during adolescence?, Journal of Psychiatric Research. 17 (1982) 319–334. https://doi.org/10.1016/0022-3956(82)90038-3.

[19] M.S. Keshavan, S. Anderson, J.W. Pettergrew, Is Schizophrenia due to excessive synaptic pruning in the prefrontal cortex? The Feinberg hypothesis revisited, Journal of Psychiatric Research. 28 (1994) 239–265. https://doi.org/10.1016/0022-3956(94)90009-4.

[20] T.H. McGlashan, R.E. Hoffman, Schizophrenia as a Disorder of Developmentally Reduced Synaptic Connectivity, Archives of General Psychiatry. 57 (2000) 637–648.

[21] I.N. Karatsoreos, Links between Circadian Rhythms and Psychiatric Disease, Front Behav Neurosci. 8 (2014) 162. https://doi.org/10.3389/fnbeh.2014.00162.

[22] P. Jia, G. Han, J. Zhao, P. Lu, Z. Zhao, SZGR 2.0: a one-stop shop of schizophrenia candidate genes, Nucleic Acids Res. 45 (2017) D915–D924. https://doi.org/10.1093/nar/gkw902.

[23] P. Trepte, A. Buntru, K. Klockmeier, L. Willmore, A. Arumughan, C. Secker, M. Zenkner, L. Brusendorf, K. Rau, A. Redel, E.E. Wanker, DULIP: A Dual Luminescence-Based Co-Immunoprecipitation Assay for Interactome Mapping in Mammalian Cells, J Mol Biol. 427 (2015) 3375–3388. https://doi.org/10.1016/j.jmb.2015.08.003.

[24] P. Trepte, S. Kruse, S. Kostova, S. Hoffmann, A. Buntru, A. Tempelmeier, C. Secker, L. Diez, A. Schulz, K. Klockmeier, M. Zenkner, S. Golusik, K. Rau, S. Schnoegl, C.C. Garner, E.E. Wanker, LuTHy: a double-readout bioluminescence-based two-hybrid technology for quantitative mapping of protein–protein interactions in mammalian cells, Molecular Systems Biology. 14 (2018). https://doi.org/10.15252/msb.20178071.

[25] K. Blaszczyk, H. Nowicka, K. Kostyrko, A. Antonczyk, J. Wesoly, H.A.R. Bluyssen, The unique role of STAT2 in constitutive and IFN-induced transcription and antiviral responses, Cytokine & Growth Factor Reviews. 29 (2016) 71–81. https://doi.org/10.1016/j.cytogfr.2016.02.010.

[26] K. Honda, T. Taniguchi, IRFs: master regulators of signalling by Toll-like receptors and cytosolic pattern-recognition receptors, Nature Reviews Immunology. 6 (2006) 644–658. https://doi.org/10.1038/nri1900.

[27] N. Müller, E. Weidinger, B. Leitner, M.J. Schwarz, The role of inflammation in schizophrenia, Front Neurosci. 9 (2015). https://doi.org/10.3389/fnins.2015.00372.

[28] G. Yachdav, E. Kloppmann, L. Kajan, M. Hecht, T. Goldberg, T. Hamp, P. Hönigschmid, A. Schafferhans, M. Roos, M. Bernhofer, L. Richter, H. Ashkenazy, M. Punta, A. Schlessinger, Y. Bromberg, R. Schneider, G. Vriend, C. Sander, N. Ben-Tal, B. Rost, PredictProtein—an open resource for online prediction of protein structural and functional features, Nucleic Acids Res. 42 (2014) W337–W343. https://doi.org/10.1093/nar/gku366.

[29] H.J. Williams, N. Norton, S. Dwyer, V. Moskvina, I. Nikolov, L. Carroll, L. Georgieva, N.M. Williams, D.W. Morris, E.M. Quinn, I. Giegling, M. Ikeda, J. Wood, T. Lencz, C. Hultman, P. Lichtenstein, D. Thiselton, B.S. Maher, Molecular Genetics of Schizophrenia Collaboration (MGS) International Schizophrenia Consortium (ISC), SGENE-plus, GROUP, A.K. Malhotra, B. Riley, K.S. Kendler, M. Gill, P. Sullivan, P. Sklar, S. Purcell, V.L. Nimgaonkar, G. Kirov, P. Holmans, A. Corvin, D. Rujescu, N. Craddock, M.J. Owen, M.C. O'Donovan, Fine mapping of ZNF804A and genome-wide significant evidence for its involvement in schizophrenia and bipolar disorder, Mol Psychiatry. 16 (2011) 429–441. https://doi.org/10.1038/mp.2010.36.

[30] C. Schindler, D.E. Levy, T. Decker, JAK-STAT signaling: from interferons to cytokines, J Biol Chem. 282 (2007) 20059–20063. https://doi.org/10.1074/jbc.R700016200.

[31] G.R. Stark, J.E. Darnell, The JAK-STAT pathway at twenty, Immunity. 36 (2012) 503–514. https://doi.org/10.1016/j.immuni.2012.03.013.

[32] N. Raftery, N.J. Stevenson, Advances in anti-viral immune defence: revealing the importance of the IFN JAK/STAT pathway, Cell Mol Life Sci. 74 (2017) 2525–2535. https://doi.org/10.1007/s00018-017-2520-2.

[33] H.C. Steen, A.M. Gamero, STAT2 phosphorylation and signaling, JAKSTAT. 2 (2013) e25790. https://doi.org/10.4161/jkst.25790.

[34] L.M. Wakim, N. Gupta, J.D. Mintern, J.A. Villadangos, Enhanced survival of lung tissue-resident memory CD8$^+$ T cells during infection with influenza virus due to selective expression of IFITM3, Nat Immunol. 14 (2013) 238–245. https://doi.org/10.1038/ni.2525.

[35] A.R. Everitt, S. Clare, T. Pertel, S.P. John, R.S. Wash, S.E. Smith, C.R. Chin, E.M. Feeley, J.S. Sims, D.J. Adams, H.M. Wise, L. Kane, D. Goulding, P. Digard, V. Anttila, J.K. Baillie, T.S. Walsh, D.A. Hume, A. Palotie, Y. Xue, V. Colonna, C. Tyler-Smith, J. Dunning, S.B. Gordon, GenISIS Investigators, MOSAIC Investigators, R.L. Smyth, P.J. Openshaw, G. Dougan, A.L. Brass, P. Kellam, IFITM3 restricts the morbidity and mortality associated with influenza, Nature. 484 (2012) 519–523. https://doi.org/10.1038/nature10921.

[36] A.S. Brown, Epidemiologic studies of exposure to prenatal infection and risk of schizophrenia and autism, Dev Neurobiol. 72 (2012) 1272–1276. https://doi.org/10.1002/dneu.22024.

[37] A.S. Brown, E.J. Derkits, Prenatal infection and schizophrenia: a review of epidemiologic and translational studies, Am J Psychiatry. 167 (2010) 261–280. https://doi.org/10.1176/appi.ajp.2009.09030361.

[38] A.S. Brown, M.D. Begg, S. Gravenstein, C.A. Schaefer, R.J. Wyatt, M. Bresnahan, V.P. Babulas, E.S. Susser, Serologic evidence of prenatal influenza in the etiology of schizophrenia, Arch Gen Psychiatry. 61 (2004) 774–780. https://doi.org/10.1001/archpsyc.61.8.774.

[39] M.J. Gandal, P. Zhang, E. Hadjimichael, R.L. Walker, C. Chen, S. Liu, H. Won, H. van Bakel, M. Varghese, Y. Wang, A.W. Shieh, J. Haney, S. Parhami, J. Belmont, M. Kim, P. Moran Losada, Z. Khan, J. Mleczko, Y. Xia, R. Dai, D. Wang, Y.T. Yang, M. Xu, K. Fish, P.R. Hof, J.

Warrell, D. Fitzgerald, K. White, A.E. Jaffe, PsychENCODE Consortium, M.A. Peters, M. Gerstein, C. Liu, L.M. Iakoucheva, D. Pinto, D.H. Geschwind, Transcriptome-wide isoform-level dysregulation in ASD, schizophrenia, and bipolar disorder, Science. 362 (2018). https://doi.org/10.1126/science.aat8127.

[40] E. Platanitis, D. Demiroz, A. Schneller, K. Fischer, C. Capelle, M. Hartl, T. Gossenreiter, M. Müller, M. Novatchkova, T. Decker, A molecular switch from STAT2-IRF9 to ISGF3 underlies interferon-induced gene transcription, Nature Communications. 10 (2019) 2921. https://doi.org/10.1038/s41467-019-10970-y.

[41] R.K. Singh, J. Shi, B.W. Zemaitaitis, N.A. Muma, Olanzapine increases RGS7 protein expression via stimulation of the Janus tyrosine kinase-signal transducer and activator of transcription signaling cascade, J Pharmacol Exp Ther. 322 (2007) 133–140. https://doi.org/10.1124/jpet.107.120386.

[42] N. Bhana, R.H. Foster, R. Olney, G.L. Plosker, Olanzapine, Drugs. 61 (2001) 111–161. https://doi.org/10.2165/00003495-200161010-00011.

[43] U. Stelzl, U. Worm, M. Lalowski, C. Haenig, F.H. Brembeck, H. Goehler, M. Stroedicke, M. Zenkner, A. Schoenherr, S. Koeppen, J. Timm, S. Mintzlaff, C. Abraham, N. Bock, S. Kietzmann, A. Goedde, E. Toksöz, A. Droege, S. Krobitsch, B. Korn, W. Birchmeier, H. Lehrach, E.E. Wanker, A Human Protein-Protein Interaction Network: A Resource for Annotating the Proteome, Cell. 122 (2005) 957–968. https://doi.org/10.1016/j.cell.2005.08.029.

[44] A. Boeddrich, J.T. Babila, T. Wiglenda, L. Diez, M. Jacob, W. Nietfeld, M.R. Huska, C. Haenig, N. Groenke, A. Buntru, E. Blanc, J.C. Meier, E. Vannoni, C. Erck, B. Friedrich, H. Martens, N. Neuendorf, S. Schnoegl, D.P. Wolfer, M. Loos, D. Beule, M.A. Andrade-Navarro, E.E. Wanker, The Anti-amyloid Compound DO1 Decreases Plaque Pathology and Neuroinflammation-Related Expression Changes in 5xFAD Transgenic Mice, Cell Chemical Biology. 26 (2019) 109-120.e7. https://doi.org/10.1016/j.chembiol.2018.10.013.

Figures and Figure captions:
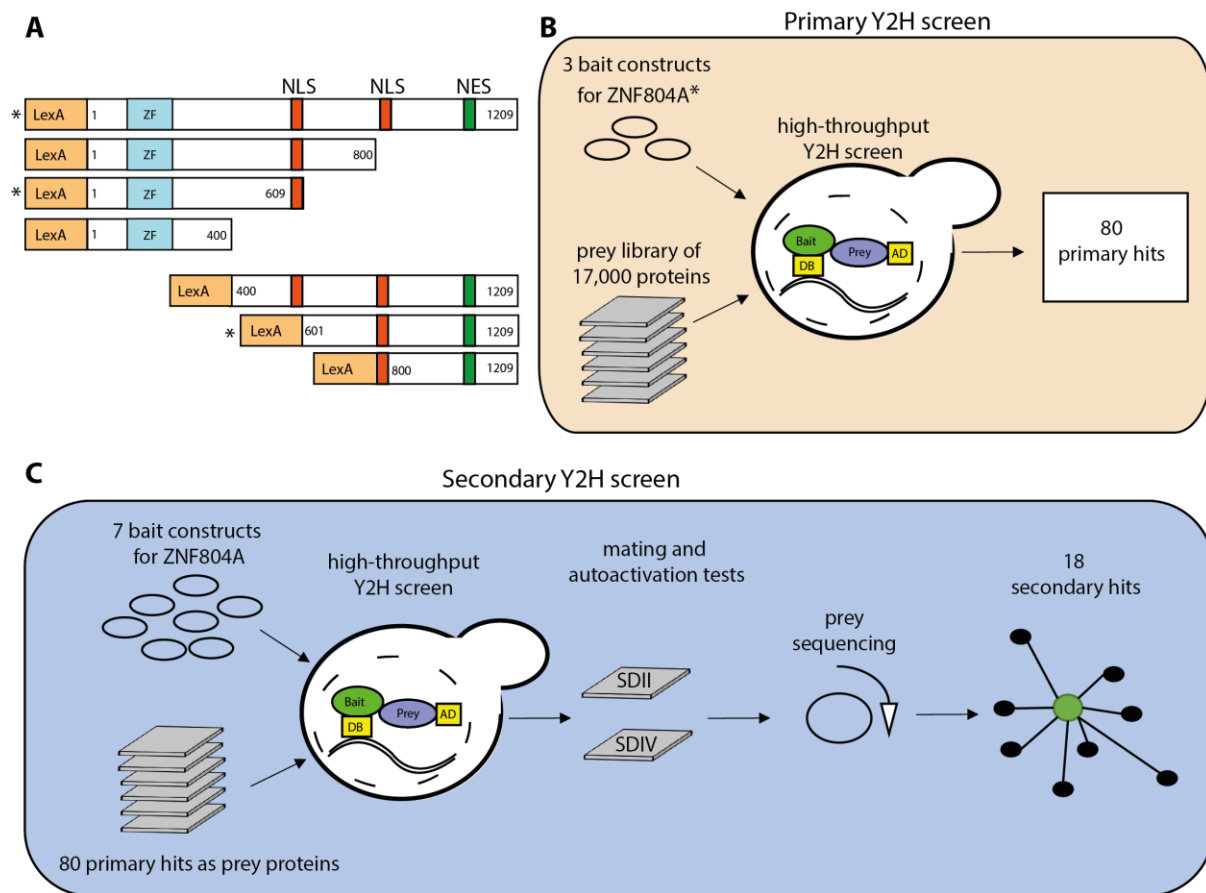
Figure 1: Yeast two-hybrid screening of ZNF804A protein-protein interactors. (A) Overview of ZNF804A bait constructs used in Y2H screens. Asterisks represent bait constructs used in the primary Y2H screen. Orange, LexA tag; blue, ZF, zinc-finger domain; red, NLS, nuclear localization sequence; green, NES, nuclear export sequence. (B) Schematic representation primary Y2H screen. Asterisk represents bait constructs used in the primary Y2H screen shown in (A). (C) Schematic representation secondary Y2H screen. All seven baits shown in (A) were used in this screen against 84 primary prey hits. Secondary screen included additional mating and autoactivation tests, followed by prey sequencing.
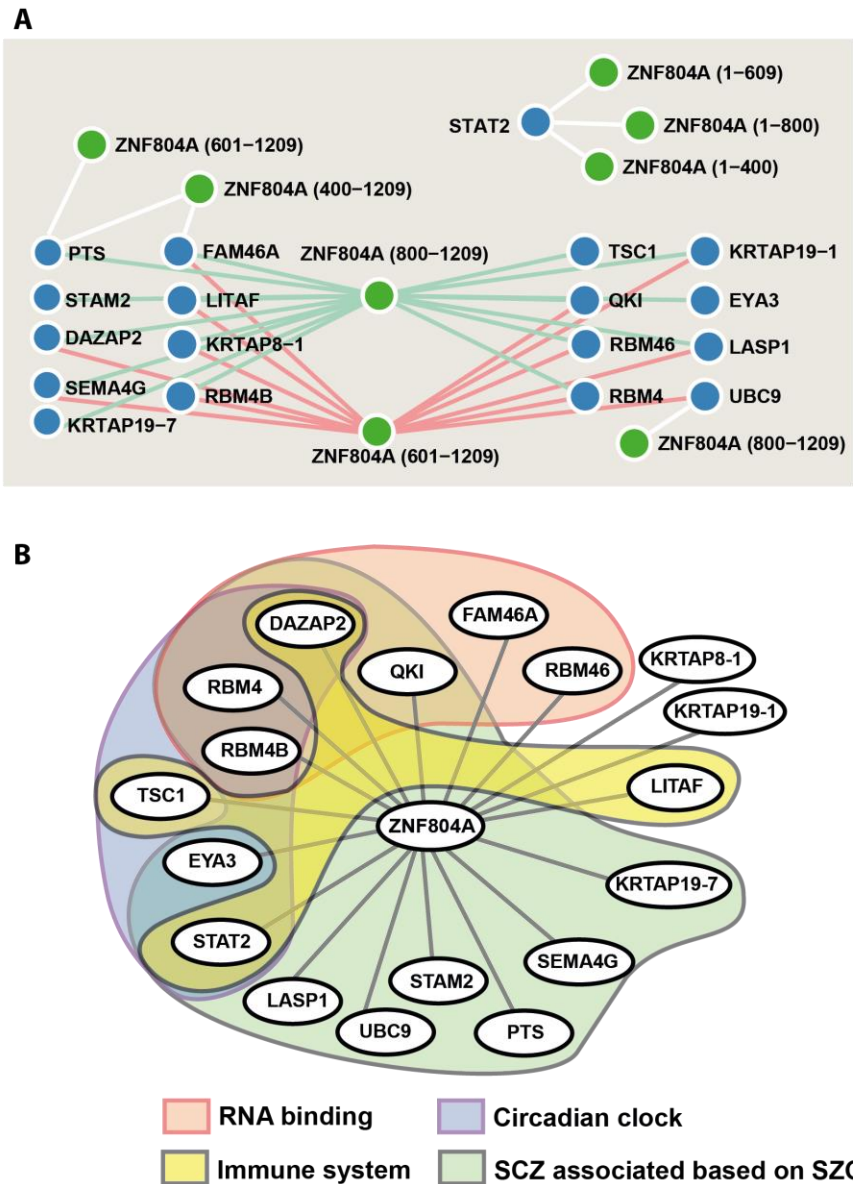
Figure 2: Yeast two-hybrid screening identifies 18 ZNF804A interactors. (A) Mapping of the 18 interactors to the respective ZNF804A fragment for which it was found positive in the secondary Y2H screen. (B) Manual annotation of ZNF804A interaction network. Three major groups of proteins were identified with related functional annotations. Beige: RNA binding function. Purple: functional role in circadian clock/rhythm. Light blue: Associated with SZ.
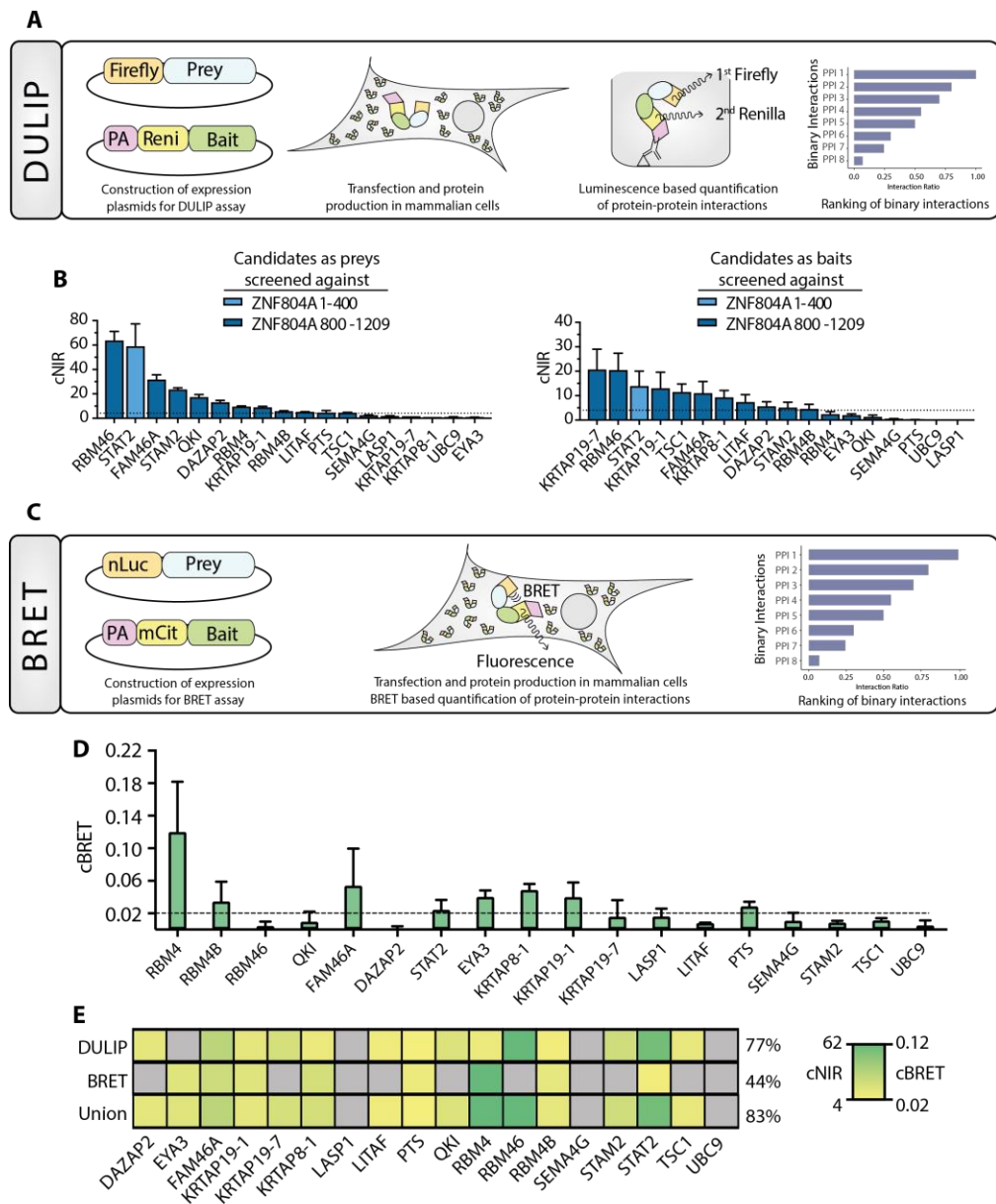
Figure 3: DULIP and BRET assays validate 12 ZNF804A interactors. (A) Workflow of DULIP validation of ZNF804A PPI interactions. HEK293 cells were transfected with bait and prey constructs; cells were lysed after 48 hours and lysates subjected to immunoprecipitation of PA-tagged proteins. Sequential luminescence readouts (first Firefly, followed by Renilla) were performed and corrected normalized interaction ratios (cNIRs) calculated. (B) DULIP cNIR values for ZNF804A fragments ZNF804A 1-400 and ZNF804A 800-1209 screened against Y2H positive hits. Values are displayed as a bar diagram (means ± SEM of three biological replicates). PPIs surpassing the cNIR threshold of 4 (dotted line) are considered positive. (C)

Schematic of BRET screening. HEK293 cells were co-transfected with plasmids for full-length ZNF804A-NanoLuC or PA-mCitrine fused to PPI candidates. After a 48 hr incubation, mCitrine fluorescence was measured followed by total luminescence and BRET readouts in living cells. Measurements were used to determine the corrected BRET ratio (cBRET). (C) cBRET values for ZNF804A interactions. Values are displayed as a bar diagram (means ± SEM of three biological replicates). PPIs surpassing the cBRET threshold of 0.02 (dotted line) were considered positive. (E) Summary of DULIP and BRET screening as a heatmap. The DULIP row represents the maximum cNIR value derived from the prey and bait screening from (B). The Union category represents the relative higher interaction score from DULIP and BRET experiments. Coloring indicates interaction strength, specified by cNIR and cBRET values (yellow to green). Grey coloring indicates interactions below the significant threshold as stated in (B) and (D). Numbers on the right-hand side of heatmap represent percentage of validated proteins.

Figure 4: STAT2 exhibits multiple interaction sites to ZNF804A. (A) Western blot validation of anti-STAT2 (sc-476) specificity for STAT2 in cell lysates transfected with plasmids encoding GFP fused STAT family proteins. Endogenous and STAT2-GFP are observed in the blot. (B) Increasing amounts of recombinant His tagged STAT2 isolated from bacteria was subjected to

western blotting. Recombinant protein was detected with anti-STAT2 antibody (sc-476). (C) Representative peptide array of the first 400 amino acids of ZNF804A and IRF9 (amino acids 205-393) were incubated with recombinant His-STAT2 (20 µM) and binding of STAT2 detected with STAT2 antibody. Sequence of spotted peptides are displayed in Supplementary Table 3. Dash lines represents no peptide spotting. (D) cBRET values for full-length (FL) and ZNF804A fragment 1-400 screened against STAT2 fused with mCitrine. ZNF804A constructs lacking the zinc-finger domain (ΔZF) were also tested. PPIs surpassing the cBRET threshold of 0.02 (dotted line) are considered positive. Data represent means ± SEM of three biological replicates. One-way ANOVA, Tukey's multiple comparison test; n.s not significant. (E) Quantification of spot intensities from four independent experiments (background-corrected mean intensities ± STD). One-way ANOVA, Tukey's multiple comparison test; ***, $P < 0.001$. (F) Analysis of the first 400 amino acids of ZNF804A using GenScript peptide property calculator tool. Indicated are the zinc-finger domain, as well as the three strong STAT2 peptide spotting regions from (E). Colors indicate polarity of amino acids; blue: basic residues (R, K and H); green: hydrophobic uncharged residues (F, I, L, M, V, W, A and P); red: acidic residues (D and E); grey: other residues (G, S, T, C, N, Q and P). Value next to highlighted peptides represents the iso-electric point in pH. (G) Evaluation of structured regions using PredictProtein.org analysis tools. Helix, Strands, and disordered regions are shown. Zinc-finger domain and the three strong STAT2 peptide spotting regions from (E) are also represented.
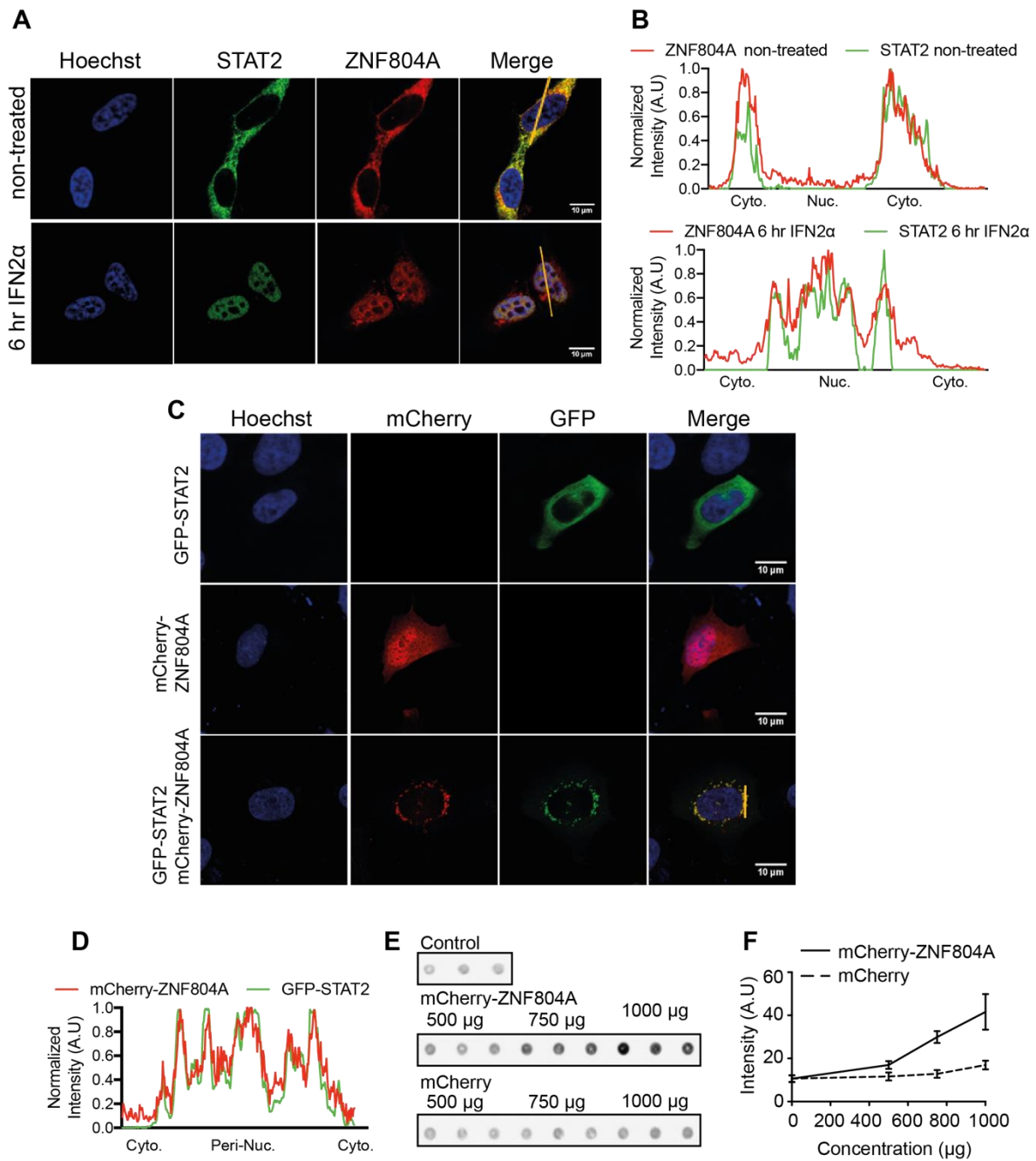
Figure 5: STAT2 and ZNF804A translocate into the nucleus upon IFN2α stimulation. (A)

Representative confocal images of SHEP cells stained with Hoechst (blue) for nuclear staining,

anti-STAT2 (green) and anti-ZNF804A (red). Yellow lines indicate the selected region for line

scan analysis. (B) Line scan analysis based on intensity profiles of STAT2 and ZNF804A of non-

treated and IFN2α-treated shown in (A). Highest measured intensity was set to 1. Cyto,

cytoplasmic and Nuc, Nuclear. (C) Representative confocal images of SHEP cells transfected

with GFP-STAT2, mCherry-ZNF804A plasmids or both co-transfected. Yellow line indicates the selected region for line scan analysis. (D) Line scan analysis based on intensity profiles of GFP-STAT2 and mCherry-ZNF804A shown in (C). Highest measured intensity was set to 1. (E) Representative denaturing filter retardation membrane of HEK293 cells transfected with 1000 µg STAT2 and 1000 µg empty vector (top) or STAT2 co-transfected with increasing amounts of either mCherryZNF804A (middle) or mCherry alone (bottom). Each spot represents an independent sample. (F) Quantification of filter retardation membrane, n = 3 independent biological samples. Error bars represent STD.
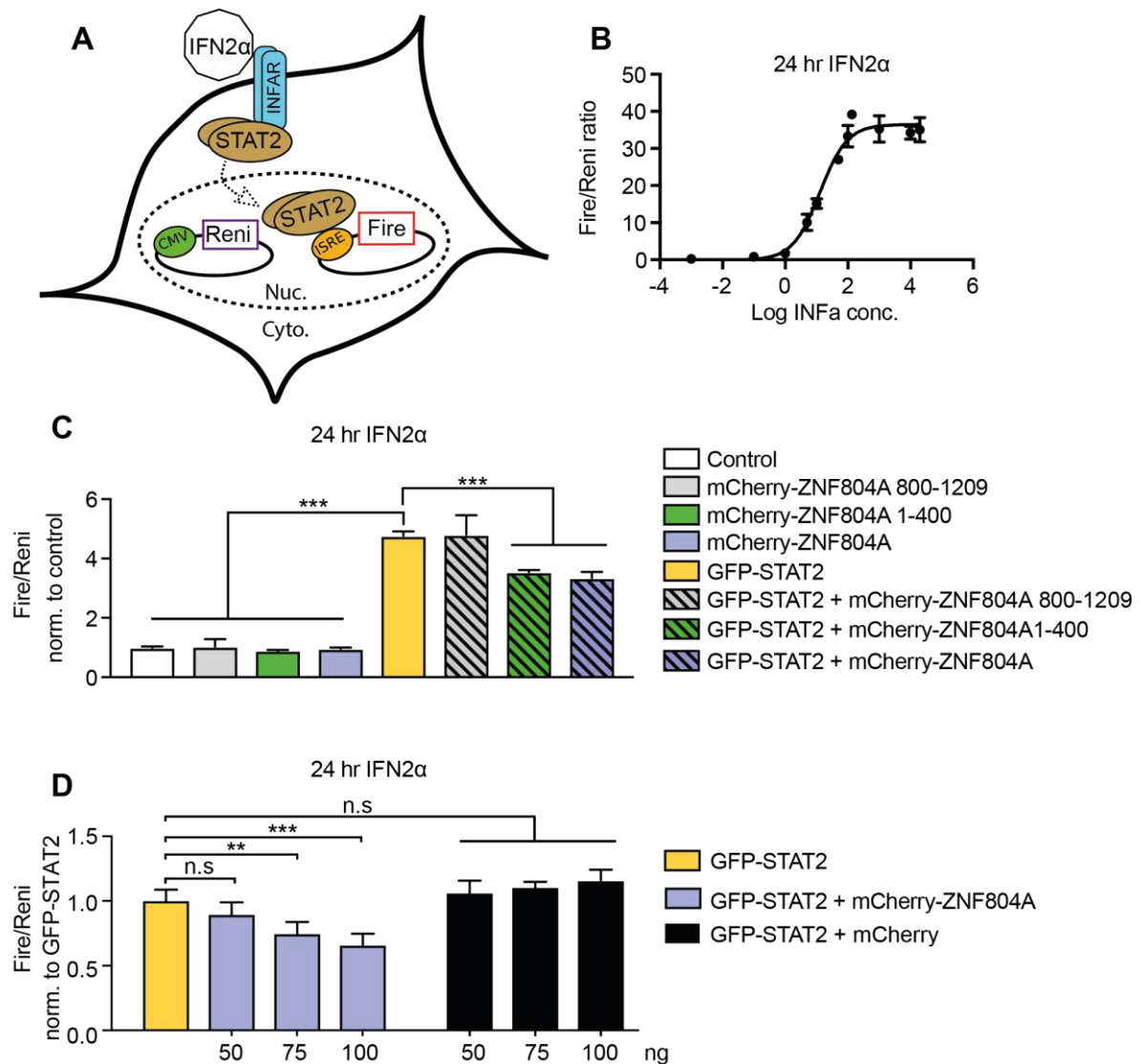
Figure 6: Overexpression of ZNF804A attenuates STAT2-mediated ISRE response. (A) Scheme of ISRE reporter response assay. HEK293 cells were co-transfected with constructively expressed CMV Renilla luciferase and ISRE-dependent expression of Firefly luciferase. Upon IFN2α stimulation, IFN2a activation leads to activation of STAT2 which binds to the ISRE promoter allowing for Firefly expression. The ratio of Firefly/Renilla was calculated and used to assess ISRE binding and activation. Cyto, cytoplasm; Nuc, nucleus. (B) ISRE reporter response performed with increasing IFN2α concentrations. Values are displayed as ratios of Firefly luciferase (reporter) to Renilla luciferase (control). n = 3 biological replicates. (C) ISRE reporter response measurements in HEK293 cells transfected with 100 ng of empty
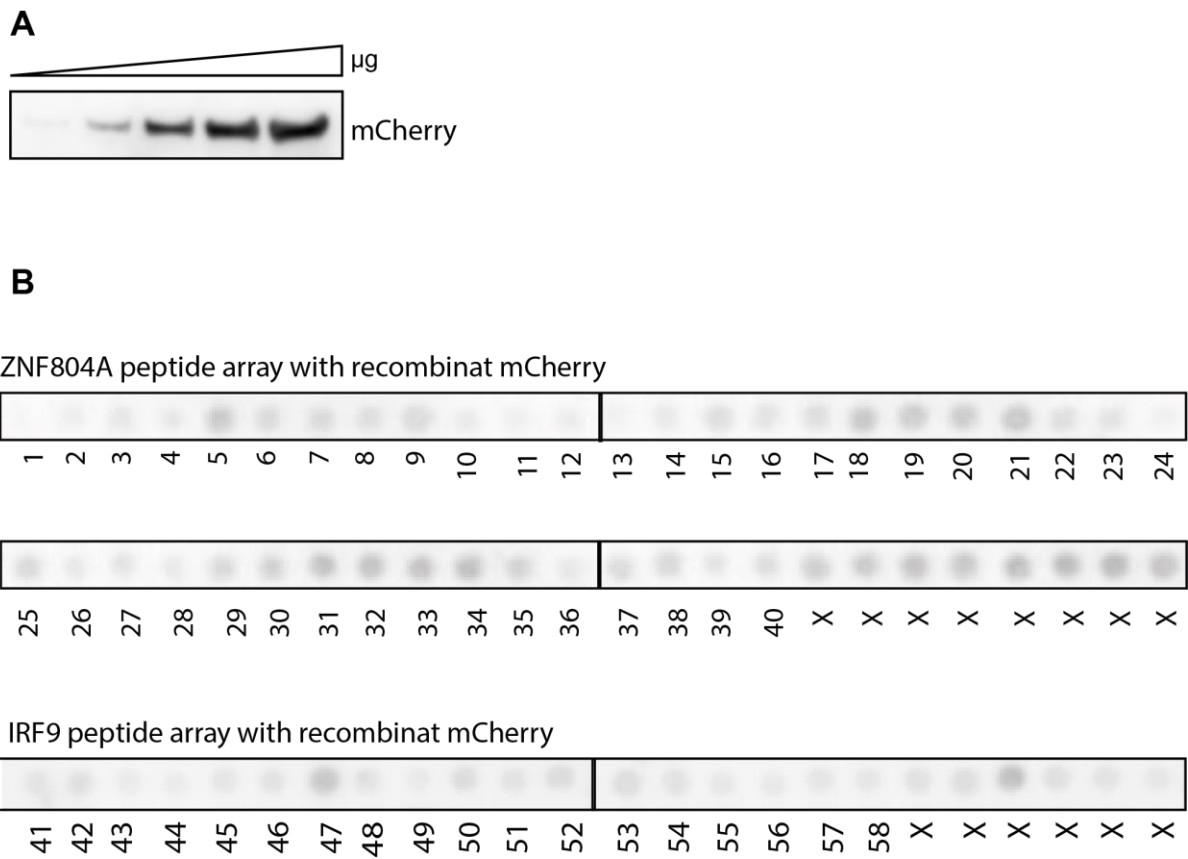
mCherry vector, mCherry-ZNF804A 1-400, mCherry-ZNF804A 800-1209, or full-length ZNF804A. HEK293 cells were also transfected with 100 ng of GFP-STAT2 alone or GFP-STAT2 co-transfected with, mCherry-ZNF804A 800-1209, mCherry-ZNF804A 1-400, or full-length ZNF804A. Cells were treated with 50 U/ml of IFN2α for 24 hours before ISRE measurements. n = 3-8 biological replicates. (D) ISRE reporter response measurements in HEK293 cells transfected with 100 ng of GFP-STAT2 or co-transfected with increasing amounts of full-length ZNF804A or empty mCherry vector. Cells were treated with 50 U/ml of IFN2α for 24 hours before ISRE measurements. n = 2-9 biological replicates. For all, error bars represent STD. One-way ANOVA, Dunnett's multiple comparison test; *, $P < 0.05$; **, $P < 0.01$; ***, $P < 0.001$, n.s. non-significant.
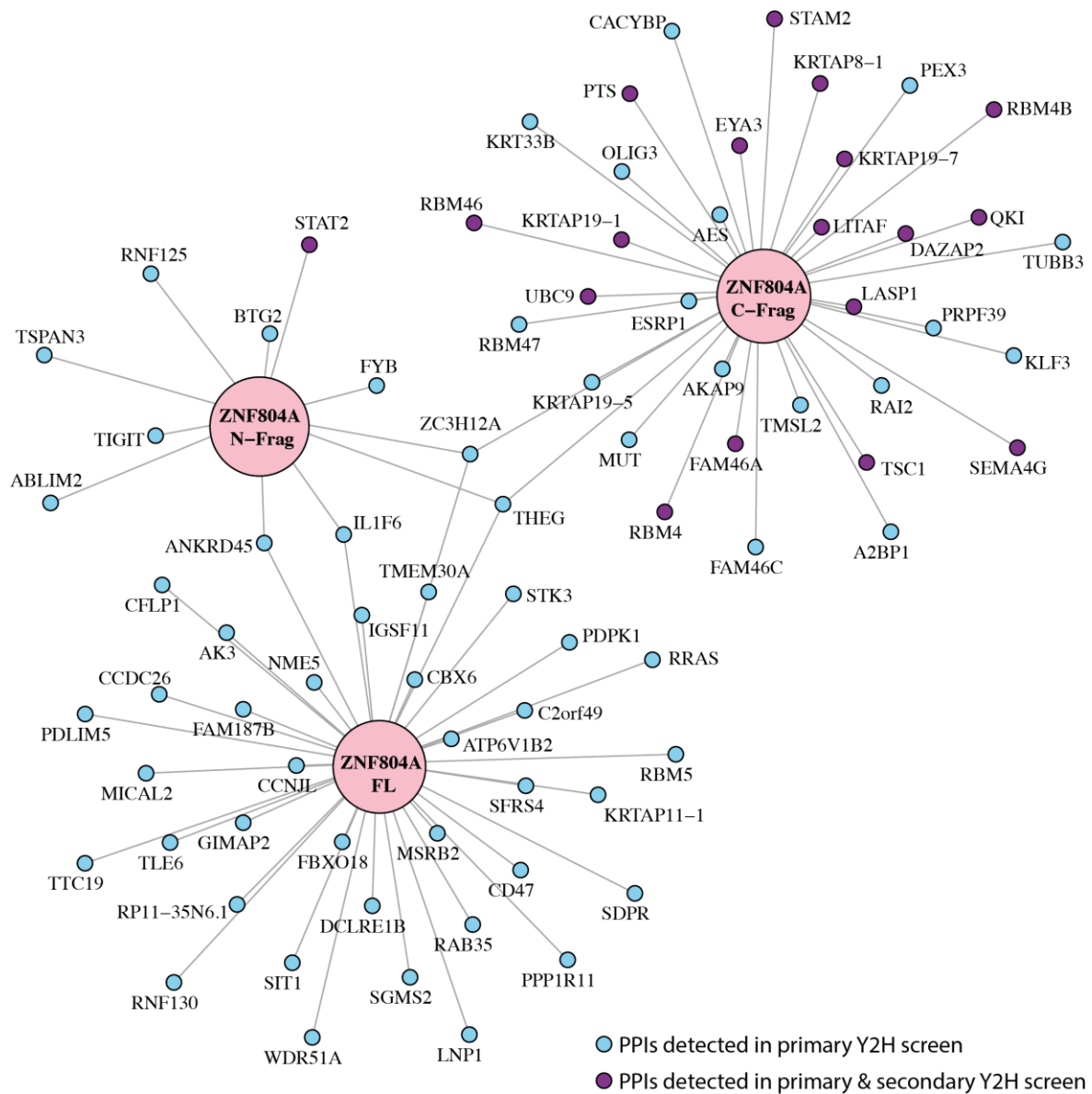
Supplementary figure 1: Interaction mapping of hits from the primary Y2H screen. The 80
Y2H hits from the primary Y2H screen with a positive confidence score were mapped to the
respective ZNF804A bait. 11 proteins were positive with N-terminal ZNF804A, 34 proteins
interacted with C-terminal ZNF804A, and 35 proteins interacted with full-length ZNF804A.
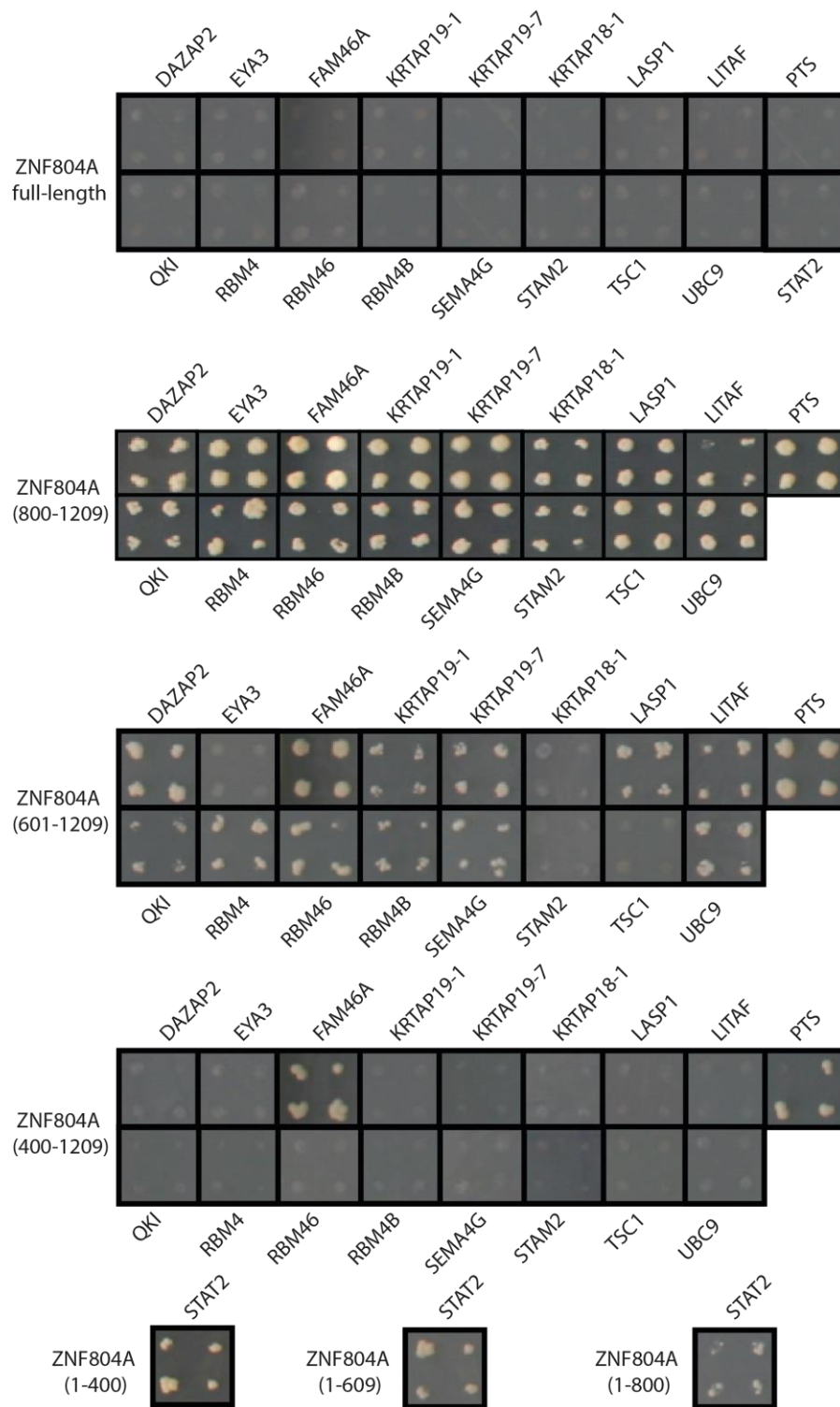
Supplementary figure 2: **Y2H colony growth on SDIV plates**. Representative images of quadruplicate colonies of the 18 Y2H hits from the secondary Y2H screen. The respective ZNF804A bait (full-length or fragment) in which the PPI was detected is shown. A PPI was considered positive if three out of the four colonies showed growth.

A

µg

mCherry

B

ZNF804A peptide array with recombinat mCherry

1 2 3 4 5 6 7 8 9 10 11 12 13 14 15 16 17 18 19 20 21 22 23 24

25 26 27 28 29 30 31 32 33 34 35 36 37 38 39 40 X X X X X X X X

IRF9 peptide array with recombinat mCherry

41 42 43 44 45 46 47 48 49 50 51 52 53 54 55 56 57 58 X X X X X X

Supplementary figure 3: **Peptide Arrays with mCherry**. (A) Increasing amounts of recombinant His tagged mCherry isolated from bacteria was subjected to western blotting. Recombinant mCherry protein was detected with anti-mCherry antibody (Clonetech 632543). (B) Representative images of ZNF804A and IRF9 peptide arrays incubated with recombinant His-mCherry. X denotes spots with no peptide.